

Multi-dimensional Biochemical Information Processing of Dynamical Patterns

Yoshihiko Hasegawa*

Department of Information and Communication Engineering,
Graduate School of Information Science and Technology,
The University of Tokyo, Tokyo 113-8656, Japan

(Dated: September 25, 2018)

Cells receive signaling molecules by receptors and relay information via sensory networks so that they can respond properly depending on the type of signal. Recent studies have shown that cells can extract multi-dimensional information from dynamical concentration patterns of signaling molecules. We herein study how biochemical systems can process multi-dimensional information embedded in dynamical patterns. We model the decoding networks by linear response functions, and optimize the functions with the calculus of variations to maximize the mutual information between patterns and output. We find that, when the noise intensity is lower, decoders with different linear response functions, i.e., distinct decoders, can extract much information. However, when the noise intensity is higher, distinct decoders do not provide the maximum amount of information. This indicates that, when transmitting information by dynamical patterns, embedding information in multiple patterns is not optimal when the noise intensity is very large. Furthermore, we explore the biochemical implementations of these decoders using control theory and demonstrate that these decoders can be implemented biochemically through the modification of cascade-type networks, which are prevalent in actual signaling pathways.

I. INTRODUCTION

Cells receive signals by receptors and subsequently process the obtained information through biochemical networks so that they can respond properly. In addition to static information, such as the concentration or identity of signaling molecules, recent experimental evidence shows that cells can process dynamical patterns [1, 2]. Specifically, it was reported that biochemical networks can filter dynamical signals in order to counteract noise or for prediction [3–5]. Because one-dimensional *static* signals can be specified by a single variable (e.g., the concentration), they provide only one-dimensional information. On the other hand, one-dimensional *dynamical* signals require multi-dimensional information to specify their shape, and hence they are multi-dimensional. The extraction of the dynamical patterns lets cells learn more about the environment. For multicellular organisms, dynamical patterns are used for inter-cellular communication. A biophysical example of inter-cellular information transmission using dynamic patterns is insulin [2]. Based on experiments, it has been reported that multiple messages are embedded in dynamical patterns and that each specific pattern is selectively decoded by their downstream molecular networks [6–8]. One notable advantage of using dynamical patterns for communications over static patterns is considered to be the ability to encode more information into a common molecular species [9]. Although cellular dynamical information processing has attracted much attention [3–17], very little attention has been paid to the multi-dimensional aspects of the information processing of dynamical patterns [9, 18, 19].

Here, we study how biochemical systems can optimally extract multi-dimensional information from dynamical patterns. Considering the deterministic limit of decoders (vanishing intrinsic noise limit), we can describe their response by linear response functions (Fig. 1(a)). For dynamical signals with two basis functions and two types of decoders, we obtain an optimal linear response function through the calculus of variations in order to maximize mutual information between dynamical patterns and output. We find that decoders with different linear response functions (*distinct* decoders) can achieve optimal extraction of the information from dynamical patterns. However, when the noise intensity is excessively high, the use of decoders with the same linear response function (*identical* decoders) can extract more information than the use of distinct decoders. Using control theory, we also show that these optimal decoders can be implemented biochemically by a cascade-type linear signaling network with additional feedforward and feedback loops, which are prevalent in actual signaling pathways.

II. MODELS

We consider a biochemical sensory system that reads out extracellular dynamical patterns by receptors, subsequently processes the signal via decoding networks, and finally reports the result as the concentration of output molecular species [Fig. 1(b)]. We assume that there exist N decoding systems, each of which consists of receptors and a subsequent decoding network [$N = 2$ for Fig. 1(b)]. In order to quantify the amount of transmitted information, we need to define the probability density on dynamical patterns. As each dynamical pattern has infinite dimensions, the definition of their probability density function is not trivial. We model a dynamical pattern $w(t)$

*Electronic address: hasegawa@biom.t.u-tokyo.ac.jp

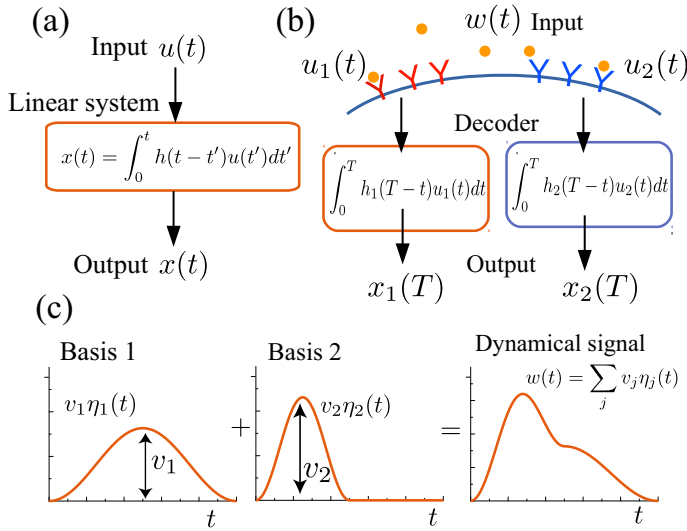


FIG. 1: (a) Relation between input $u(t)$ and output $x(t)$ in a linear system through linear response function $h(t)$. (b) Decoding of dynamical patterns by two decoding systems. Input signal $w(t)$ is received by N types of receptors, and the signal is processed by subsequent internal molecular decoders ($N = 2$ in this figure). The linear response function of the i th decoder is given by $h_i(t)$. Each decoder outputs results by $x_i(T)$. (c) Dynamical pattern $w(t)$ as a sum of basis functions $\eta_j(t)$ at intensities v_j .

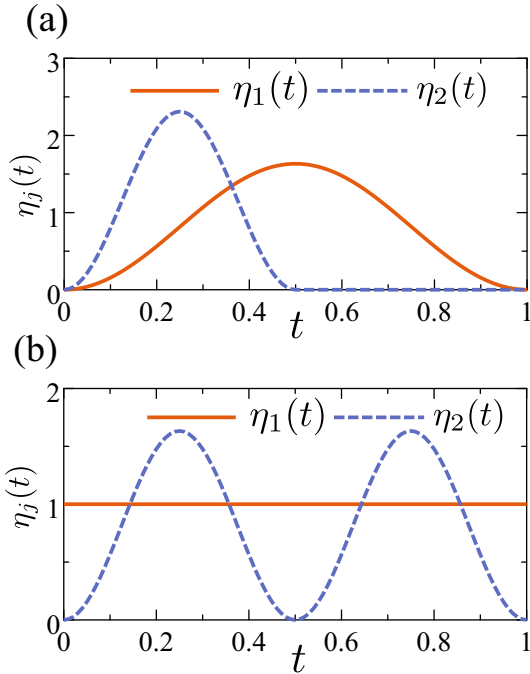


FIG. 2: Basis sets for the $M = 2$ case [solid and dashed lines denote $\eta_1(t)$ and $\eta_2(t)$, respectively]. (a) Slow and fast patterns (basis set A). (b) Constant and oscillation patterns (basis set B).

by a sum of basis functions after Ref. [20]:

$$w(t) = \sum_{j=1}^M v_j \eta_j(t), \quad (1)$$

where M is the number of basis functions, $\boldsymbol{\eta}(t) = [\eta_1(t), \dots, \eta_M(t)]$ are basis functions, and $\boldsymbol{v} = [v_1, \dots, v_M]$ are their coefficients, which are referred to as intensities. Figure 1(c) describes the model, where a dynamical pattern $w(t)$ is composed of two basis functions, $\eta_1(t)$ and $\eta_2(t)$. The basis functions need not be orthogonal. However, except for a particular case of I^{dup} considered later herein, the basis functions should be linearly independent. We define probability density $P(\boldsymbol{v})$ on \boldsymbol{v} , which are used to define the probability density of the dynamical patterns. Although Eq. (1) is introduced to incorporate the probability density on dynamical patterns, the basis functions $\eta_j(t)$ and their number M have direct biological interpretations for some intercellular communication. Cells can decode multiplexed dynamical patterns [1, 2, 6, 8, 13, 15], where the patterns can be broadly classified into two basic dynamics, fast pulsatile and slow transient patterns. Cells can read out amplitude information embedded in the two patterns. In this example, the number of basis functions is $M = 2$, and $\eta_1(t)$ and $\eta_2(t)$ correspond to the fast and slow patterns.

We assume that $\eta_j(t)$ is in a steady state for $t < 0$, where we define $\eta_j(t) = 0$ for the steady state concentration (and hence $w(t) = 0$ for $t < 0$), and $w(t)$ starts to change at time $t = 0$. Due to stochasticity, accompanied by, e.g., stochastic receptor-ligand binding, each decoder reads out a degraded pattern $u_i(t)$:

$$u_i(t) = w(t) + \xi_i(t),$$

where $\xi_i(t)$ is the input noise of the i th type of receptors, defined by $\langle \xi_i(t) \rangle = 0$, and $\langle \xi_i(t) \xi_{i'}(t') \rangle = 2D_i \delta_{ii'} \delta(t-t')$, where D_i is the noise intensity. The noise intensity D_i depends primarily on the number of i th-type receptors and the dissociation constant of the binding-unbinding reaction [21]. Moreover the dissociation constant has a temperature dependence via the van't Hoff equation.

Next, we model the dynamics of the decoders. Let $x_i(t)$ be the output concentration of the i th decoder at time t , and, for $t < 0$, we define $x_i(0) = 0$. Note that $w(t)$ and $x_i(t)$ are concentrations relative to steady state and so can take negative values. In order to make analytic calculation possible, we consider a deterministic limit of decoders [5, 22]. Decoders consist of biochemical reactions subject to intrinsic noise, the concentration dynamics of which can be described by stochastic processes. If we consider an infinitely large number of molecules while keeping the concentration constant, intrinsic noise vanishes and the stochastic processes reduce to deterministic differential equations, which is referred to as the deterministic limit. We assume that decoders output results after a finite time $t = T$ (for simplicity, we set the same time interval for each decoder), and so

$\mathbf{x}(T) = [x_1(T), \dots, x_N(T)]$ contain information on the dynamical pattern. Suppose that the i th decoder is the single-layer linear decoder (linear birth-death process) given by

$$\dot{z}_i(t) = -\theta_i z_i + u_i(t), \quad (2)$$

where $z_i(t)$ is the concentration of molecular species in the i th decoder, and θ_i is the degradation rate. In this decoder, $z_i(t)$ directly reports the result, i.e., $x_i(T) = z_i(T)$. A similar model was proposed for decoding calcium oscillation [23]. Because of the linearity of Eq. (2), the output at time t is given by a convolution integral:

$$x_i(t) = \int_0^t h_i(t-t')u_i(t')dt', \quad (3)$$

where $h_i(t)$ is the linear response function. For this single-layer and linear case, $h_i(t) = e^{-\theta_i t}$. Biochemical decoders are often composed of multiple layers, which can yield complex linear response functions $h_i(t)$ [cf. Eq. (13)] [4, 5, 22]. For arbitrary linear response functions, the average at $t = T$ is $\mu_{x_i} = \langle x_i(T) \rangle = \int_0^T h_i(T-t')w(t')dt'$, and the variance is $\sigma_{x_i}^2 = 2D_i \int_0^T h_i(t')^2 dt'$ [20] (see Appendix A). Although we used $x(T)$ as the output of the decoders in the present model, based on Eq. (3), $x(T)$ can also be regarded as the (weighted) time integration of some intermediate concentration.

Let $x_i^T = x_i(T)$, which is output of the i th decoder at time $t = T$. The amount of information contained in the output $\mathbf{x}^T = [x_1^T, x_2^T, \dots, x_N^T]$ is quantified by the mutual information

$$I[\mathbf{x}^T; \mathbf{v}] = \int d\mathbf{x}^T \int d\mathbf{v} P(\mathbf{x}^T|\mathbf{v})P(\mathbf{v}) \ln \left[\frac{P(\mathbf{x}^T|\mathbf{v})}{P(\mathbf{x}^T)} \right]. \quad (4)$$

Here, $P(\mathbf{x}^T|\mathbf{v})$ is the probability density of \mathbf{x}^T given \mathbf{v} , and $P(\mathbf{v})$ is the probability density on $\mathbf{v} = [v_1, \dots, v_M]$. Equation (4) is the quantity defined between \mathbf{x} at time $t = T$ and \mathbf{v} . We assume independent probability densities for v_j , $P(\mathbf{v}) = \prod_{j=1}^M P(v_j)$, where $P(v_j)$ is the Gaussian distribution with mean μ_j and variance $\sigma_{v_j}^2$. Although we assumed independence for v_j , we can eliminate this assumption when \mathbf{v} is distributed according to a multivariate Gaussian distribution. If \mathbf{v} has a multivariate Gaussian distribution, we can apply a linear transform to redefine basis functions $\boldsymbol{\eta}(t)$ so that elements of \mathbf{v} become uncorrelated with each other (see Appendix B). Since uncorrelated Gaussian random variables are independent, we can always make the independence assumption for \mathbf{v} .

We wish to find optimal decoders which maximally extract information from dynamical patterns. Instead of exploring all possible candidate structures, we optimize a set of linear response functions $\mathbf{h}(t) = [h_1(t), \dots, h_N(t)]$ with the calculus of variations. Thus we obtain a desirable biochemical system through an optimization problem with an identifiable objective function [24–26].

Taking into account biological situations, we consider the following three optimization problems (itali-

cized words in parentheses are abbreviations): (i) maximization of $I[\mathbf{x}^T; \mathbf{v}]$ (*full decoder*), (ii) maximization of $I[\mathbf{x}^T; \mathbf{v}]$ with $P(\mathbf{x}^T) = \prod_i P(x_i^T)$ (*decorrelating decoder*), and (iii) maximization of $I[\mathbf{x}^T; \mathbf{v}]$ with single-layer linear decoders (*SLL decoder*). For (i), decoders obtained by full maximization provide an upper bound on the mutual information between dynamical patterns and output. When cells want to extract as much information as possible, this maximization is suitable. For (ii), $P(\mathbf{x}^T) = \prod_i P(x_i^T)$ can be easily incorporated into the maximization if $N = M$, which is assumed here. As the input noises $\boldsymbol{\xi}(t) = [\xi_1(t), \dots, \xi_N(t)]$ affect each receptor independently (Fig. 1(b)), we have $P(\mathbf{x}^T|\mathbf{v}) = \prod_{i=1}^N P(x_i^T|\mathbf{v})$. Combining these relations, we arrive at

$$\begin{aligned} P(\mathbf{x}^T) &= \int d\mathbf{v} P(\mathbf{x}^T|\mathbf{v})P(\mathbf{v}), \\ &= \int d\mathbf{v} \prod_{i=1}^N P(x_i^T|\mathbf{v}) \prod_{j=1}^{N(=M)} P(v_j). \end{aligned}$$

If each $P(x_i^T|\mathbf{v})$ disjointly depends on only one v_i [i.e., $P(x_i^T|\mathbf{v}) = P(x_i^T|v_i)$], we can show that $P(\mathbf{x}^T) = \prod_i P(x_i^T)$. This is similar to a decorrelator in digital communication, which decorrelates multiplexed signals (see Appendix C). For this case, v_i can be obtained by measuring only one $x_i(T)$, i.e., $I[\mathbf{x}^T; \mathbf{v}] = \sum_{i=1}^N I[x_i^T; v_i]$. For (iii), we fix the linear response function to $h_i(t) = e^{-\theta_i t}$, which corresponds to the abovementioned single-layer linear (SLL) decoder. We optimize all θ_i numerically with simulated annealing to maximize $I[\mathbf{x}^T; \mathbf{v}]$.

For arbitrary N and M (both $N = M$ and $N \neq M$ are allowed), we obtain the optimal linear response functions as follows (see Appendix C):

$$h_i(t) = -\frac{1}{4\Lambda_i D_i} \sum_{j=1}^M \lambda_{ij} \eta_j(T-t), \quad (5)$$

where λ_{ij} and Λ_i are Lagrange multipliers (real values), and these values depend on the type of decoders (full or decorrelating). When observing the dynamical pattern composed of a single basis function ($M = 1$) with a single decoder ($N = 1$), the optimal linear response function is $h_1(t) \propto \eta_1(T-t)$, which is known as the matched filter. From Eq. (5), the optimal linear response function that maximizes the mutual information is given by the summation of matched filters. Although the matched filter is known to be optimal for $M = N = 1$, the optimality of Eq. (5) for maximization of the mutual information is not trivial.

III. RESULTS

A. Mutual information

We construct concrete optimal linear response functions for a system with $N = M = 2$. In actual intercellular communication, as far as known, the degree of

multiplexing is very small. Moreover, obtaining optimal linear response functions becomes more difficult as N or M increases. Therefore, we select $N = M = 2$ as the minimal model for the multi-dimensional information processing. For the basis functions $\eta_j(t)$, we consider the two basis sets shown in Figs. 2(a) and (b). The two basis sets A and B are defined by

$$\text{Set A} \begin{cases} \eta_1(t) &= \sqrt{\frac{2}{3}}(1 - \cos(2\pi t)), \\ \eta_2(t) &= \frac{2}{\sqrt{3}}\Theta\left(\frac{1}{2} - t\right)(1 - \cos(4\pi t)), \end{cases} \quad (6)$$

and

$$\text{Set B} \begin{cases} \eta_1(t) &= 1, \\ \eta_2(t) &= \sqrt{\frac{2}{3}}(1 - \cos(4\pi t)). \end{cases} \quad (7)$$

Basis set A comprises slow and fast patterns (Fig. 2(a)), where $\Theta(t)$ is a step function; and basis set B comprises constant and oscillation patterns (Fig. 2(b)). All of the basis functions are normalized so that $\psi_{11} = 1$ and $\psi_{22} = 1$, where $\psi_{jj'}$ is the correlation matrix defined by $\psi_{jj'} = \int_0^T \eta_j(t)\eta_{j'}(t)dt$. Regarding T , it is reasonable to choose T as the largest duration time among $\eta_j(t)$. If T is shorter than the largest time, decoders cannot use all of the information contained in $w(t)$. Conversely, even if T is longer than the largest time, decoders cannot extract more information from $w(t)$. Therefore, we use $T = 1$ for both of the basis sets.

Let I^{full} , I^{decor} , and I^{sll} be the mutual information $I[\mathbf{x}^T; \mathbf{v}]$ of the full, decorrelating, and SLL decoders, respectively. I^{full} , I^{decor} , and I^{sll} are obtained by optimizing the linear response functions. As explained above, the mutual information quantities assume a model in which information is embedded in two linearly independent basis functions, is transmitted through a common channel, and is decoded by two decoders (Fig. 3(a)). We cannot obtain closed-form solutions for I^{full} and I^{sll} for arbitrary noise intensity, so we calculate the solutions numerically (see Appendix C). For sufficiently small D_1 and D_2 , I^{full} is approximated by

$$I^{\text{full}} \simeq \frac{1}{2} \ln \left(\frac{\sigma_{v_1}^2 \sigma_{v_2}^2 (\psi_{11}\psi_{22} - \psi_{12}^2)}{4D_1 D_2} \right). \quad (8)$$

When $\eta_1(t)$ and $\eta_2(t)$ are linearly independent, we have $\psi_{11}\psi_{22} > \psi_{12}^2$. I^{decor} can be calculated in closed form for arbitrary noise intensity (see Appendix C). For sufficiently small D_1 and D_2 , I^{decor} is approximated by

$$I^{\text{decor}} \simeq \frac{1}{2} \ln \left(\frac{\sigma_{v_1}^2 \sigma_{v_2}^2 (\psi_{11}\psi_{22} - \psi_{12}^2)^2}{4D_1 D_2 \psi_{11} \psi_{22}} \right). \quad (9)$$

For comparison, we consider the mutual information I^{dual} which corresponds to a model where information embedded in two basis functions is transmitted through

two designated channels and is decoded by two designated decoders (Fig. 3(b)). Applying the calculus of variations, I^{dual} is represented by

$$I^{\text{dual}} = I[x_1^T; v_1] + I[x_2^T; v_2], \\ = \frac{1}{2} \ln \left(1 + \frac{\sigma_{v_1}^2 \psi_{11}}{2D_1} \right) + \frac{1}{2} \ln \left(1 + \frac{\sigma_{v_2}^2 \psi_{22}}{2D_2} \right). \quad (10)$$

Note that I^{dual} does not have biological relevance but is introduced merely as a theoretical reference point. From Eqs. (8) and (10), when D_1 and D_2 are sufficiently small, the following relation holds:

$$I^{\text{full}} \leq I^{\text{dual}}, \quad (11)$$

where it holds with equality when the correlation between the two basis functions is zero (i.e., $\psi_{12} = 0$).

Figures 4(a) and (b) show I^{full} , I^{decor} , I^{sll} , and I^{dual} (solid, dashed, dotted, and dot-dashed lines, respectively) as functions of the noise intensity D ($= D_1 = D_2$) for basis sets A and B, respectively. Parameter details are shown in the caption of Fig. 4. In Figs. 4(a) and (b), we see that I^{full} and I^{decor} yield higher values than I^{sll} for a lower noise intensity D , especially in Fig. 4(a), which indicates that optimal linear response functions extract information more efficiently than SLL decoders. The insets in Figs. 4(a) and (b) highlight $I^{\text{dual}} - I^{\text{full}}$ as a function of D . Interestingly, for large noise intensity D , the two mutual information quantities I^{full} and I^{dual} obey $I^{\text{full}} > I^{\text{dual}}$, which is the opposite relation to Eq. (11) (Eq. (11) is satisfied for sufficiently *small* D). This relation is nontrivial because the use of designated channels, which corresponds to I^{dual} , is expected to provide higher information transmission, as shown by Eq. (11).

In order to investigate the cause of this opposite relation between I^{full} and I^{dual} with respect to D , we examine the optimal response functions, which are shown in Fig. 5. Figures 5(a) and (b) show linear response functions $h_1(t)$ (solid line) and $h_2(t)$ (dashed line) for the full decoder with basis set A for different noise intensities ($D = 0.1$ and 1.0 , respectively) while keeping the other parameters unchanged (details are shown in the caption of Fig. 5). Note that for $D < 0.1$, the shapes of the optimal linear response functions are similar to that of $D = 0.1$, and for $D > 1.0$, the shapes are similar to that of $D = 1.0$. In Fig. 5(c), we also show the optimal linear response functions $h_1(t)$ (solid line) and $h_2(t)$ (dashed line) for the decorrelating decoder. In this case, there is no major difference when noise intensity D is varied. We can see that for $D = 0.1$ (Fig. 5(a)), the linear response function of the full decoder is similar to that of the decorrelating decoder of Fig. 5(c), indicating that the decorrelation can provide near-optimal efficiency for the weak-noise case. In Fig. 5(a), $h_i(t)$ indicated by solid and dashed lines mainly decode information embedded in slow and fast patterns, respectively. When we increase D in the fully optimal case, the two linear response functions coalesce to a single function (the critical points are $D \simeq 0.83$ for basis set A and $D \simeq 0.20$ for basis set

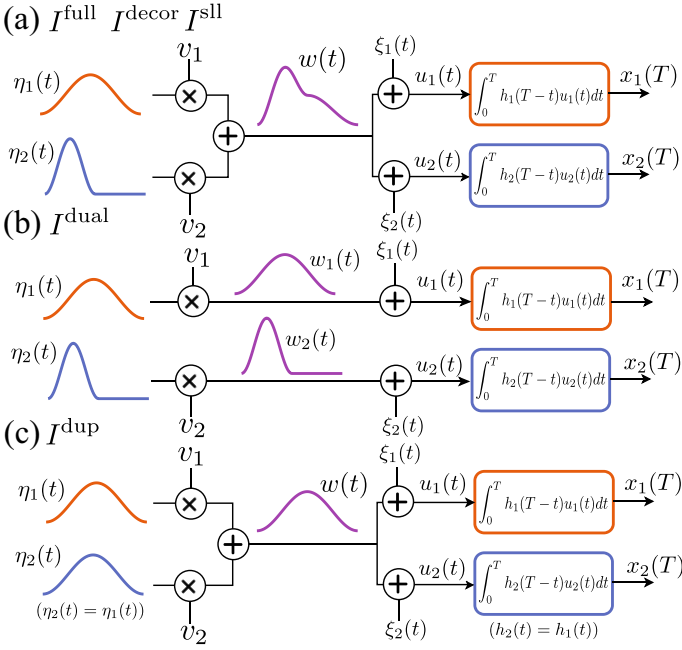


FIG. 3: Information transmission model assumed in different mutual information. (a) Information is embedded in two distinct basis functions, transmitted through one common channel, and decoded by two decoders. (b) Information is embedded in two distinct basis functions, transmitted through two designated channels, and decoded by two decoders. (c) Information is embedded in two identical basis functions, transmitted through one channel, and decoded by two identical decoders. In (a)–(c), \oplus and \otimes denote addition and multiplication operations, respectively.

B). This result indicates that, when the noise intensity is very strong, decoding information with two distinct decoders is inefficient but decoding with identical decoders is relatively efficient. Therefore, in the region in which I^{full} and I^{dual} obey $I^{\text{dual}} < I^{\text{full}}$, a qualitative change in the linear response functions occurred.

In order to explain this change in great detail, we introduce another mutual information quantity I^{dup} , which assumes a model similar to that shown in Fig. 3(a) but uses the same function for the two basis functions ($\eta_1(t) = \eta_2(t)$) and the same linear response function for the two decoders ($h_1(t) = h_2(t)$), as shown in Fig. 3(c). We also set $D_1 = D_2 = D$ and $\sigma_{v_1}^2 = \sigma_{v_2}^2 = \sigma_v^2$. Optimizing the linear response functions, I^{dup} is given by (see Appendix C)

$$I^{\text{dup}} = \frac{1}{2} \ln \left(1 + \frac{2\sigma_v^2 \psi}{D} \right), \quad (12)$$

where $\psi = \psi_{11} = \psi_{22}$. Figure 4(c) shows I^{dual} and I^{dup} as functions of D , and we observe that $I^{\text{dual}} > I^{\text{dup}}$ for weaker noise intensity, while $I^{\text{dup}} > I^{\text{dual}}$ for larger noise intensity. This indicates that when the noise intensity is excessively large, multi-dimensional information transmission becomes inefficient. Transmitting information by

embedding information into two identical basis functions and decoding using two identical decoders becomes more efficient.

B. Biochemical implementation

We next explore a biochemical implementation of the optimal decoders. We attempt to implement a decoding network corresponding to $h_i(t)$ with K_i molecular species (K_i is determined by the degree of the transfer function; see below). Linearizing around the steady state, we describe their dynamics by the following linear model:

$$\dot{\mathbf{z}}_i(t) = \mathbf{A}_i \mathbf{z}_i(t) + \mathbf{b}_i u_i(t). \quad (13)$$

where $\mathbf{z}_i(t) = [z_{i1}(t), \dots, z_{iK_i}(t)]^\top$, $z_{ik}(t)$ is the relative concentration of the k th molecular species in the i th decoder, \mathbf{A}_i is a $K_i \times K_i$ matrix, and \mathbf{b}_i is a K_i -dimensional column vector. The output of Eq. (13) is $z_{iK_i}(t)$ and hence $x_i(T) = z_{iK_i}(T)$ (the last molecular species reports the result). Independent of the type of maximization (the full or decorrelating decoders), from Eq. (5), Laplace transform yields

$$\tilde{h}_i(s) = -\frac{1}{4\Lambda_i D_i} \sum_{j=1}^M \lambda_{ij} \tilde{\eta}_j(s), \quad (14)$$

where $\tilde{h}_i(s) = \mathcal{L}[h_i(t)]$ (the transfer function) and $\tilde{\eta}_j(s) = \mathcal{L}[\tilde{\eta}_j(T-t)]$ with \mathcal{L} being the Laplace transform. We want to identify \mathbf{A}_i and \mathbf{b}_i which yield the desired transfer functions $\tilde{h}_i(s)$. This problem is known as the realization problem in control theory [27]. Let the transfer function be a rational polynomial function of the form

$$\tilde{h}_i(s) = \frac{\sum_{k=1}^{K_i} \beta_{ik} s^{K_i-k}}{s^{K_i} + \sum_{k=1}^{K_i} \alpha_{ik} s^{K_i-k}}, \quad (15)$$

where β_{ik} and α_{ik} are real values, and the degree of the denominator is larger than that of the nominator (this condition is called *strictly proper*). From control theory, one possible realization of this transfer function is (see Appendix D)

$$\mathbf{A}_i = \begin{bmatrix} 0 & 0 & 0 & \cdots & -\alpha_{iK_i} \\ 1 & 0 & 0 & \cdots & -\alpha_{i,K_i-1} \\ 0 & 1 & 0 & \cdots & -\alpha_{i,K_i-2} \\ \vdots & \vdots & \vdots & \ddots & \vdots \\ 0 & 0 & 0 & 1 & -\alpha_{i1} \end{bmatrix}, \quad \mathbf{b}_i = \begin{bmatrix} \beta_{iK_i} \\ \beta_{i,K_i-1} \\ \beta_{i,K_i-2} \\ \vdots \\ \beta_{i1} \end{bmatrix}. \quad (16)$$

Off-diagonal ones in Eq. (16) imply that z_{ik} depends on $z_{i,k-1}$ ($k = 2, 3, \dots, K_i$), which corresponds to a cascade topology. When the transfer function is strictly proper, its corresponding linear systems can be implemented by a cascade network with additional feedback and feed-forward loops. As is well known, the cascade topology is prevalent in actual signaling networks and additional

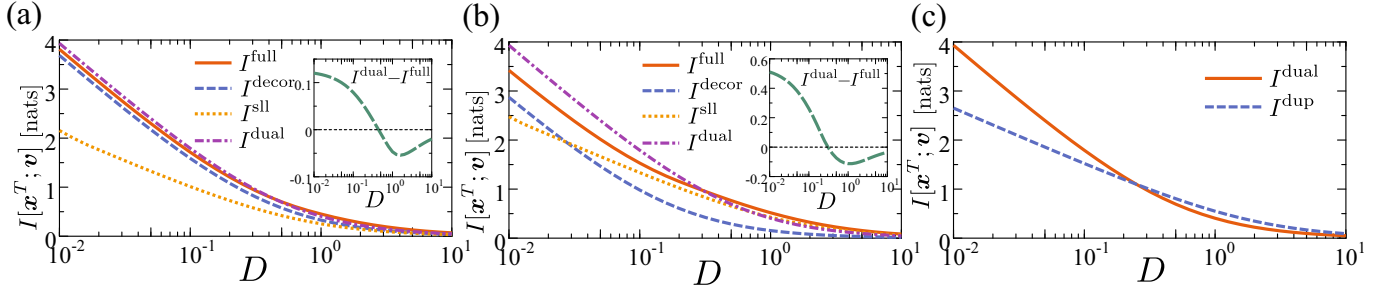


FIG. 4: (a) and (b) Mutual information as a function of noise intensity D by basis set; (a) basis set A [Fig. 2(a)] and (b) basis set B [Fig. 2(b)]. Solid, dashed, dotted, and dot-dashed lines denote I^{full} , I^{decor} , I^{sll} , and I^{dual} , respectively. In (a) and (b), the insets highlight $I^{\text{dual}} - I^{\text{full}}$ as a function of D . (c) Mutual information quantities I^{dual} (solid line) and I^{dup} (dashed line) as functions of D . Note that I^{dual} and I^{dup} do not depend on the basis set. In all panels, parameters are $T = 1$ and $\sigma_{v_1}^2 = \sigma_{v_2}^2 = 1$.

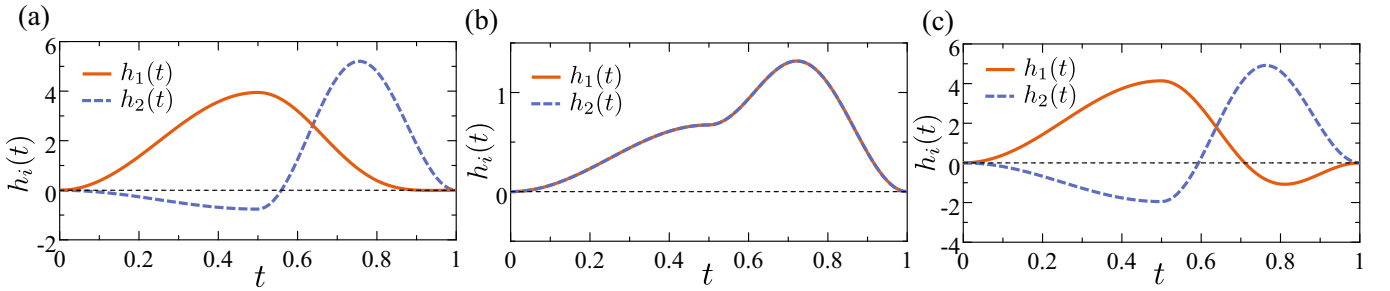


FIG. 5: (a) and (b) Optimal linear response function $h_i(t)$ of the full decoder with basis set A for different noise intensities; (a) $D = 0.1$ and (b) $D = 1.0$, where all other parameters are the same. (c) Optimal linear response function $h_i(t)$ of the decorrelating decoder with $D = 0.1$. In all panels, the solid and dashed lines denote $h_1(t)$ and $h_2(t)$, respectively. For all $h_i(t)$ shown, the functions that are horizontally symmetric with respect to $h_i = 0$ are also optimal solutions. We set $\sigma_{x_1}^2 = \sigma_{x_2}^2 = 1$, and these parameters affect only the magnitude of the functions. The other parameters are identical to those in Fig. 4.

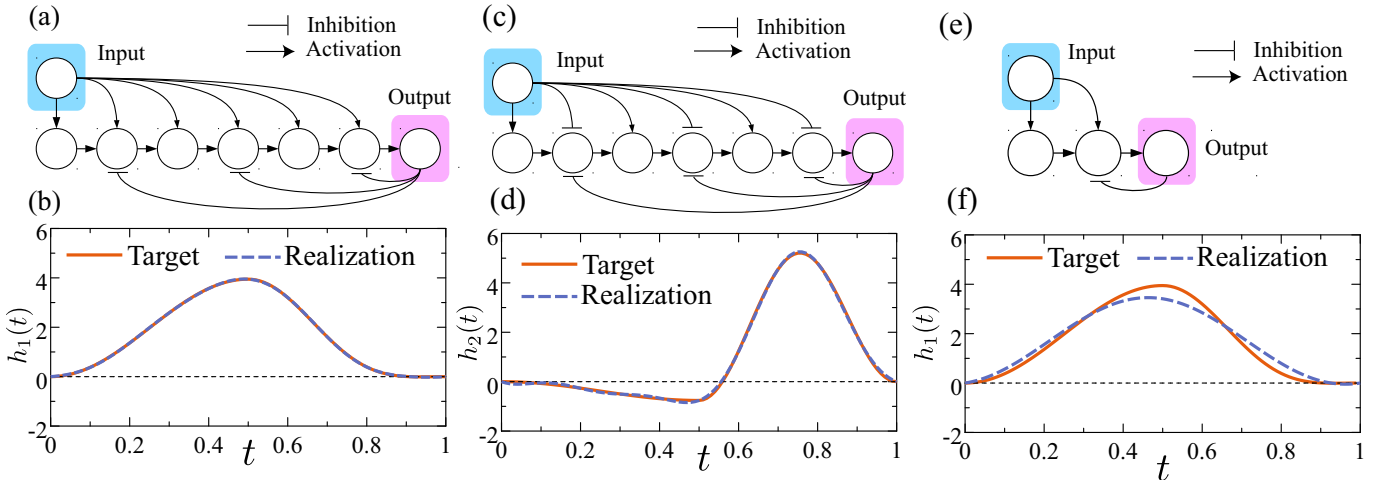


FIG. 6: (a) Molecular realization of $h_1(t)$ in Fig. 5(a), and (b) its linear response function. In (a), arrows and bar-headed arrows denote activation and inhibition, respectively. In (b), the dashed line is the linear response function of the realization network and the solid line is the target optimal linear response function shown in Fig. 5(a). (c) Molecular realization of $h_2(t)$ in Fig. 5(a) and (d) its linear response function. (e) Reduced molecular realization for the full network shown in Fig. 6(a) and (f) its linear response function. In (c)–(f), the meanings of the arrows and lines are the same as in (a) and (b).

feedback and feedforward loops exists in the networks, implying that it is possible to implement optimal decoders biochemically.

As an example, we construct biochemical implementations for the decoders of the basis set \mathbf{A} with $D = 0.1$ (Fig. 5(a)). We show the biochemical networks in Figs. 6(a) and (c), which are realizations of $h_1(t)$ and $h_2(t)$ in Fig. 5(a), respectively. Figures 6(b) and (d) show linear response functions of the networks in Figs. 6(a) and (c), respectively. The realization networks are created by applying the Fourier series expansion to $\eta_j(t)$ and calculating their Laplace transform (see Appendix D). In Figs. 6(a) and (c), when matrix elements of \mathbf{A}_i and \mathbf{b}_i are positive or negative, we display their relation by activation (arrow) or inhibition (bar-headed arrow), respectively. In Figs. 6(b) and (d), we can see that the linear response functions of the molecular networks (dashed line) are indistinguishable from the target optimal linear response function $h_i(t)$ (solid line). This indicates that the biochemical networks which maximally exploit information from dynamical patterns can be implemented. The network in Fig. 6(c) decodes the fast pattern, while that in Fig. 6(a) decodes the slow pattern. The main difference between these two networks is that the latter has an incoherent feed-forward loop (iFFL) [28, 29], while the former does not. Reference [7] indicated that, when decoding temporal insulin patterns, a decoding network having an iFFL is responsive against a fast pulsatile pattern, while it does not respond to a slow ramp pattern. Because transfer functions $\tilde{h}_1(s)$ and $\tilde{h}_2(s)$ are sums of $\tilde{\eta}_1(s)$ and $\tilde{\eta}_2(s)$ with different weighting, they are rational polynomial functions with the same denominator unless they can be reduced. If $\tilde{h}_1(s)$ and $\tilde{h}_2(s)$ have the same denominator, \mathbf{A}_1 and \mathbf{A}_2 of these realizations become identical (cf. Eqs. (15) and (16)) and this is a reason why the realization networks of Figs. 6(a) and (c) have the same feedback structure from the output. Both of the implementations have 7 nodes (i.e., $K_1 = K_2 = 7$). However, we note that the molecular networks can be minimized without losing much of their response. Specifically, we construct a reduced realization network for the full network shown in Fig. 6(a). Figures 6(e) and (f) show the reduced network, which consists of 3 nodes ($K_1 = 3$), and its corresponding linear response function, respectively. The meanings of the arrows in Fig. 6(e) and the lines in Fig. 6(f) are identical to those in Figs. 6(a) and (b), respectively. From Fig. 6(f), we see that the response of the reduced realization network (dashed line) is similar to that of the optimal realization network (solid line). Although the number of nodes in the reduced network (Fig. 6(e)) is smaller than in the corresponding full network (Fig. 6(a)), the basic structures are similar: there are positive feedforward loops from the input and negative feedback loops from the output, and there is no iFFL (see Appendix D). We constructed this reduced network heuristically based on the balanced truncation in control theory. It is worthwhile to develop a systematic reduction procedure, which would lead to feasible biochemical

implementations.

IV. CONCLUDING REMARKS

In this manuscript, we considered the optimal decoding of dynamical patterns through maximization of mutual information between input and output. We found that when the noise intensity is relatively low, the distinct decoders can extract much information, as expected. On the other hand, when the noise intensity is very high, distinct decoders cannot achieve the optimal extraction of the information, while identical decoders can. Although multiplexing is naturally considered to confer higher information transmission, our results show that this is not necessarily true for the case in which receptors are subject to strong noise. Still, we note that when decoding information with the identical decoders, it is impossible to demultiplex dynamical signals. Therefore, the decoders can determine the intensity of v_1 or v_2 but cannot identify whether the intensity corresponds to v_1 or v_2 . As indicated by several experiments, cells use multiplexed dynamical patterns to transmit information. If the primary goal of cellular sensory networks is transmitting as much information as possible, our results can provide insight into a possible range of the noise intensity. Furthermore, we investigated the possibility of biochemical implementation of the optimal decoders and found that such optimal decoders can be implemented by a modification of the cascade network.

Recently, extensive research has been conducted in order to construct relations between thermodynamic cost and mutual information [30], especially in biological contexts [31, 32]. In particular, Ref. [33] studied the thermodynamic cost of the mutual information between receptors and readouts using a Markov process. Our model considers the deterministic limit and hence it ignores the intrinsic thermal noise. When we incorporate the effect of intrinsic noise, the mutual information between patterns and output should be bounded above by some thermodynamic cost. Exploration of this topic is left for future research.

Acknowledgments

This work was supported by KAKENHI Grant No. 16K00325 from the Ministry of Education, Culture, Sports, Science and Technology.

Appendix A: Mean and variance of output

We calculate the mean and the variance of output of the i th decoder as follows. As described in the main text, we can express the output of the i th decoder by Eq. (3).

The mean at time $t = T$ is

$$\begin{aligned}\mu_{x_i} &= \langle x_i(T) \rangle, \\ &= \int_0^T h_i(T-t') \langle w(t') + \xi_i(t') \rangle dt', \\ &= \int_0^T h_i(T-t') w(t') dt', \\ &= \sum_{j=1}^M v_j q_{ij},\end{aligned}\quad (\text{A1})$$

where we define

$$q_{ij} = \int_0^T h_i(T-t') \eta_j(t') dt'. \quad (\text{A2})$$

Similarly, the variance at time $t = T$ is given by

$$\begin{aligned}\sigma_{x_i}^2 &= \langle x_i(T)^2 \rangle - \langle x_i(T) \rangle^2, \\ &= \int_0^T dt' \int_0^T dt'' h_i(T-t') h_i(T-t'') \langle \xi_i(t') \xi_i(t'') \rangle, \\ &= 2D_i \int_0^T h_i(t')^2 dt'.\end{aligned}\quad (\text{A3})$$

Appendix B: Independence of \mathbf{v}

We can make elements in $\mathbf{v} = [v_1, \dots, v_M]$ independent of each other through a change of basis functions $\boldsymbol{\eta}(t) = [\eta_1(t), \dots, \eta_M(t)]$. We define a covariance matrix $\mathbf{C} = \langle \mathbf{v}^\top \mathbf{v} \rangle$, the elements of which are

$$C_{ij} = \langle v_i v_j \rangle = \int v_i v_j P(v_i, v_j) dv_i dv_j,$$

where we assumed $\langle v_j \rangle = 0$. Because the covariance matrix \mathbf{C} is real symmetric, it can be diagonalized by an

orthogonal matrix \mathbf{Q} :

$$\mathbf{D} = \mathbf{Q}^\top \mathbf{C} \mathbf{Q},$$

where \mathbf{D} is a diagonal matrix (diagonal elements are eigenvalues of \mathbf{C}). Considering a change of basis functions $\boldsymbol{\eta}'(t)^\top = \mathbf{Q}^\top \boldsymbol{\eta}(t)^\top$, a new coefficient vector $\mathbf{v}'^\top = \mathbf{Q}^\top \mathbf{v}^\top$ has a diagonal covariance matrix:

$$\langle \mathbf{v}'^\top \mathbf{v}' \rangle = \langle \mathbf{Q}^\top \mathbf{v}^\top \mathbf{v} \mathbf{Q} \rangle = \mathbf{Q}^\top \mathbf{C} \mathbf{Q} = \mathbf{D},$$

showing that elements in \mathbf{v}' are decorrelated. When \mathbf{v} obeys the multivariate Gaussian distribution, elements in \mathbf{v}' are independent of each other. Note that we cannot make arbitrary random variables independent of each other by a change of basis functions.

Appendix C: Optimal linear response function

According to the Gaussian assumption of probability density of x_i^T (x_i at time $t = T$), we have

$$P(x_i^T | \mathbf{v}) = \frac{1}{\sqrt{2\pi\sigma_{x_i}^2}} \exp\left(-\frac{(x_i^T - \sum_{j=1}^M v_j q_{ij})^2}{2\sigma_{x_i}^2}\right). \quad (\text{C1})$$

As assumed in the main text, the probability distribution of v_j is given by

$$P(v_j) = \frac{1}{\sqrt{2\pi\sigma_{v_j}^2}} \exp\left(-\frac{v_j^2}{2\sigma_{v_j}^2}\right). \quad (\text{C2})$$

The mutual information is defined by Eq. (4). For $N = M = 2$ which is considered in the manuscript, with Eqs. (C1) and (C2), the mutual information $I[\mathbf{x}^T; \mathbf{v}]$ is given by:

$$I[x_1^T, x_2^T; v_1, v_2] = \frac{1}{2} \ln \left[1 + \frac{q_{11}^2 \sigma_{v_1}^2 + q_{12}^2 \sigma_{v_2}^2}{\sigma_{x_1}^2} + \frac{q_{21}^2 \sigma_{v_1}^2 + q_{22}^2 \sigma_{v_2}^2}{\sigma_{x_2}^2} + \frac{\sigma_{v_1}^2 \sigma_{v_2}^2 (q_{11} q_{22} - q_{12} q_{21})^2}{\sigma_{x_1}^2 \sigma_{x_2}^2} \right]. \quad (\text{C3})$$

We calculate optimal linear response function $h_i(t)$ which maximizes the mutual information $I[\mathbf{x}^T; \mathbf{v}]$. As can be seen with Eq. (C3), the mutual information $I[\mathbf{x}^T; \mathbf{v}]$ is a function of $\mathbf{q} = [q_{ij}]$. Instead of directly maximizing $I[\mathbf{x}^T; \mathbf{v}]$, we consider a more tractable function $\mathcal{M}(\mathbf{q})$ which satisfies the following condition:

$$\operatorname{argmax}_{\mathbf{q}} I[\mathbf{x}^T; \mathbf{v}] = \operatorname{argmax}_{\mathbf{q}} \mathcal{M}(\mathbf{q}).$$

Then we consider the following performance index

$\mathcal{R}(\mathbf{q}, \mathbf{h})$:

$$\begin{aligned}\mathcal{R}(\mathbf{q}, \mathbf{h}) &= \mathcal{M}(\mathbf{q}) + \sum_{i,j} \lambda_{ij} \left(q_{ij} - \int_0^T h_i(T-t) \eta_j(t) dt \right) \\ &\quad + \sum_i \Lambda_i \left(\sigma_{x_i}^2 - 2D_i \int_0^T h_i(t)^2 dt \right),\end{aligned}\quad (\text{C4})$$

where λ_{ij} and Λ_i are the Lagrange multipliers. Note that arguments of \mathbf{q} in Eq. (C4) are scalars while \mathbf{h} are functions. Constraints corresponding to λ_{ij} and Λ_i are

derived from Eqs. (A2) and (A3), respectively. Because $I[\mathbf{x}^T; \mathbf{v}]$ is scale-invariant with respect to $h_i(t)$ and hence σ_{x_i} does not affect the mutual information, we set σ_{x_i} as constant (we set $\sigma_{x_i} = 1$ for all i in the main text). The total derivative of $\mathcal{R}(\mathbf{q}, \mathbf{h})$ is written by

$$\begin{aligned} d\mathcal{R} &= \sum_{i,j} \frac{\partial \mathcal{M}(\mathbf{q})}{\partial q_{ij}} dq_{ij} \\ &+ \sum_{i,j} \lambda_{ij} \left(dq_{ij} - \int_0^T \delta h_i(t) \eta_j(T-t) dt \right) \\ &+ \sum_i \Lambda_i \left(-4D_i \int_0^T h_i(t) \delta h_i(t) dt \right), \\ &= \sum_{i,j} \left(\frac{\partial \mathcal{M}(\mathbf{q})}{\partial q_{ij}} + \lambda_{ij} \right) dq_{ij} \\ &+ \sum_i \int_0^T \delta h_i(t) \left(- \sum_j \lambda_{ij} \eta_j(T-t) - 4D_i \Lambda_i h_i(t) \right) dt. \end{aligned} \quad (\text{C5})$$

Because, $d\mathcal{R}$ should vanish at a stationary point, we obtain the following relations:

$$\frac{\partial \mathcal{M}(\mathbf{q})}{\partial q_{ij}} + \lambda_{ij} = 0, \quad (\text{C6})$$

$$- \sum_j \lambda_{ij} \eta_j(T-t) - 4D_i \Lambda_i h_i(t) = 0. \quad (\text{C7})$$

From Eq. (C7), we obtain

$$h_i(t) = - \frac{1}{4\Lambda_i D_i} \sum_{j=1}^M \lambda_{ij} \eta_j(T-t), \quad (\text{C8})$$

which is Eq. (5). Depending on the type of decoders (full or decorrelating), λ_{ij} and Λ_i are determined (see below). Substituting Eq. (C8) into Eqs. (A2) and (A3), we have

$$q_{ij} = - \frac{1}{4\Lambda_i D_i} \sum_k \lambda_{ik} \psi_{kj}, \quad (\text{C9})$$

$$\sigma_{x_i}^2 = \frac{1}{8\Lambda_i^2 D_i} \sum_{j,k} \lambda_{ij} \lambda_{ik} \psi_{kj}, \quad (\text{C10})$$

where $[\psi_{jj'}]$ is a correlation matrix of the basis functions $\eta_j(t)$, defined by

$$\psi_{jj'} = \int_0^T \eta_j(t) \eta_{j'}(t) dt.$$

Algebraic equations (C6), (C9), and (C10) are solved with respect to \mathbf{q} , $\boldsymbol{\lambda}$, and $\boldsymbol{\Lambda}$ to obtain the maximum of $I[\mathbf{x}; \mathbf{v}]$.

1. Full decoder

According to Eq. (C3), we can use the following function for the full decoder:

$$\begin{aligned} \mathcal{M}(\mathbf{q}) &= \frac{q_{11}^2 \sigma_{v_1}^2 + q_{12}^2 \sigma_{v_2}^2}{\sigma_{x_1}^2} + \frac{q_{21}^2 \sigma_{v_1}^2 + q_{22}^2 \sigma_{v_2}^2}{\sigma_{x_2}^2} \\ &+ \frac{\sigma_{v_1}^2 \sigma_{v_2}^2 (q_{11} q_{22} - q_{12} q_{21})^2}{\sigma_{x_1}^2 \sigma_{x_2}^2}, \end{aligned} \quad (\text{C11})$$

Because it is difficult to obtain closed-form solutions for Eqs. (C6), (C9), and (C10) along with Eq. (C11), we numerically solve the equations.

When the noise intensity D_i is sufficiently weak, we find the following expression:

$$\begin{aligned} I^{\text{full}} &\simeq \frac{1}{2} \ln \left[\frac{\sigma_{v_1}^2 \sigma_{v_2}^2 (q_{11} q_{22} - q_{12} q_{21})^2}{\sigma_{x_1}^2 \sigma_{x_2}^2} \right], \\ &= \frac{1}{2} \ln \left[\frac{\sigma_{v_1}^2 \sigma_{v_2}^2 (\psi_{11} \psi_{22} - \psi_{12}^2)}{4D_1 D_2} \right], \end{aligned}$$

which is Eq. (8) in the main text.

2. Decorrelating decoder

For $N = M (= 2)$, which is considered in the manuscript, decorrelation is easily implemented. The output of the i th decoder at time $t = T$ is denoted by x_i^T and its probability density is $P(x_i^T | \mathbf{v})$ (Eq. (C1)). The relation can be represented by the Bayesian network shown in Fig. 7(a). For this case, the output probability density is not decorrelated, i.e., $P(\mathbf{x}^T) \neq \prod_i P(x_i^T)$ (note that since $P(\mathbf{x}^T)$ is the Gaussian distribution, decorrelation is equivalent to independence). When $P(x_i^T | \mathbf{v})$ disjointly depends on only one $v_j \in \mathbf{v}$ as shown in Fig. 7(b), the output probability density is decorrelated. This condition yields $q_{ij} = 0$ for $i \neq j$. We can use the following function for the decorrelating decoder:

$$\mathcal{M}(\mathbf{q}) = \frac{q_{11}^2 \sigma_{v_1}^2}{\sigma_{x_1}^2} + \frac{q_{22}^2 \sigma_{v_2}^2}{\sigma_{x_2}^2} + \frac{\sigma_{v_1}^2 \sigma_{v_2}^2 q_{11}^2 q_{22}^2}{\sigma_{x_1}^2 \sigma_{x_2}^2}. \quad (\text{C12})$$

We obtain the mutual information as follows:

$$I^{\text{decor}} = \frac{1}{2} \ln \left[1 + \frac{(\psi_{11} \psi_{22} - \psi_{12}^2) (2D_1 \psi_{22} \sigma_{v_2}^2 + 2D_2 \psi_{11} \sigma_{v_1}^2 + (\psi_{22} \psi_{11} - \psi_{12}^2) \sigma_{v_1}^2 \sigma_{v_2}^2)}{4D_1 D_2 \psi_{11} \psi_{22}} \right]. \quad (\text{C13})$$

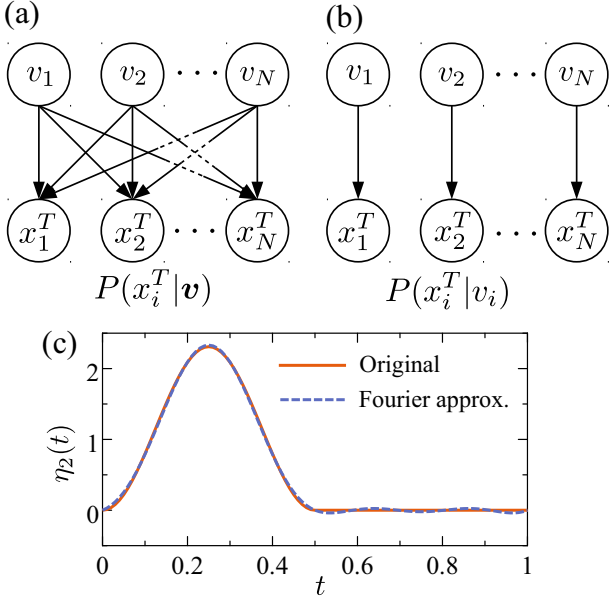


FIG. 7: (a) and (b) Network representations of (a) $P(x_i^T|\mathbf{v})$ and (b) $P(x_i^T|v_i)$ for $N = M$. (c) Basis function $\eta_2(t)$ of basis set A [Fig. 2(a)] (solid line) and its Fourier series approximation (dashed line).

When the noise intensity D_i is sufficiently weak, the mutual information reduces to Eq. (9).

3. Calculation of I^{dup}

Because $\eta_1(t) = \eta_2(t) = \eta(t)$ and $h_1(t) = h_2(t) = h(t)$ in I^{dup} , q_{ij} and $\sigma_{x_i}^2$ do not depend on i or j , where we define $q_{ij} = q$ and $\sigma_{x_i}^2 = \sigma_x^2$, respectively. Therefore, from Eq. (C3), the mutual information is

$$I[x_1^T, x_2^T; v_1, v_2] = \frac{1}{2} \ln \left(1 + \frac{4\sigma_v^2 q^2}{\sigma_x^2} \right).$$

Because $h(t) \propto \eta(T-t)$ from Eq. (C8), we have $q^2 = \psi\sigma_x^2/(2D)$ and obtain Eq. (12).

Appendix D: Network realization of transfer function

In the main text, we explore biochemical realization of optimal linear response functions $h_i(t)$. We consider a general K -dimensional linear system:

$$\dot{\mathbf{z}}(t) = \mathbf{A}\mathbf{z}(t) + \mathbf{b}u(t), \quad y(t) = \mathbf{c}\mathbf{z}(t), \quad (\text{D1})$$

where $\mathbf{z}(t)$ is a K -dimensional column vector, $y(t)$ is an output scalar variable, \mathbf{A} is a $K \times K$ matrix, \mathbf{b} is a K -dimensional column vector, and \mathbf{c} is a K -dimensional row vector. Here we dropped subscripts that identify the decoder number in order to simplify the notation (e.g., \mathbf{A}_i

in the main text is simply expressed \mathbf{A} here) because we are describing a general theory. It is known that the transfer function $\tilde{h}(s)$ of the linear system of Eq. (D1) is given by

$$\tilde{h}(s) = \mathbf{c}(s\mathbf{I} - \mathbf{A})^{-1}\mathbf{b} = \sum_{i=0}^{\infty} \frac{1}{s^{i+1}} \mathbf{c}\mathbf{A}^i\mathbf{b},$$

where \mathbf{I} is the identity matrix. Since the transfer function depends only on $\mathbf{c}\mathbf{A}^i\mathbf{b}$, the transfer function is invariant under coordinate transform $\mathbf{z}' = \mathcal{T}\mathbf{z}$, where \mathcal{T} is a regular matrix. According to the Faddeev method, $(s\mathbf{I} - \mathbf{A})^{-1}$ can be calculated by the following formula:

$$(s\mathbf{I} - \mathbf{A})^{-1} = \frac{\mathbf{F}_1 s^{K-1} + \dots + \mathbf{F}_{K-1} s + \mathbf{F}_K}{s^K + f_1 s^{K-1} + \dots + f_{K-1} s + f_K}, \quad (\text{D2})$$

where \mathbf{F}_i and f_i are defined as follows:

$$\mathbf{F}_1 = \mathbf{I}, \quad f_1 = -\text{tr}\mathbf{A}, \quad (\text{D3})$$

$$\mathbf{F}_i = \mathbf{A}\mathbf{F}_{i-1} + f_{i-1}\mathbf{I}, \quad f_i = -\frac{1}{i}\text{tr}(\mathbf{A}\mathbf{F}_i). \quad (\text{D4})$$

We consider the following rational polynomial transfer function:

$$\tilde{h}(s) = \frac{\beta_1 s^{K-1} + \dots + \beta_{K-1} s + \beta_K}{s^K + \alpha_1 s^{K-1} + \dots + \alpha_{K-1} s + \alpha_K}, \quad (\text{D5})$$

where α_i and β_i are real coefficients. One possible realization of the transfer function of Eq. (D5) in the form of Eq. (D1) is

$$\mathbf{A} = \begin{bmatrix} 0 & 0 & 0 & \dots & -\alpha_K \\ 1 & 0 & 0 & \dots & -\alpha_{K-1} \\ 0 & 1 & 0 & \dots & -\alpha_{K-2} \\ \vdots & \vdots & \vdots & \ddots & \vdots \\ 0 & 0 & 0 & 1 & -\alpha_1 \end{bmatrix}, \quad \mathbf{b} = \begin{bmatrix} \beta_K \\ \beta_{K-1} \\ \beta_{K-2} \\ \vdots \\ \beta_1 \end{bmatrix}, \quad (\text{D6})$$

and $\mathbf{c} = [0 \ 0 \ \dots \ 0 \ 1]$, which is known as the observer canonical form. Because of \mathbf{c} in Eq. (D6), the output is given by the last variable $y(t) = z_K(t)$.

In the main text, we consider network realization for basis set A, whose basis functions are given in Eq. (6). Since the step function yields a transfer function that does not fit into the form of Eq. (D5), we apply the Fourier series expansion to $\eta_2(t)$ to obtain

$$\eta_2(t) = \frac{16 \sin(2\pi t)}{3\sqrt{3}\pi} - \frac{16 \sin(6\pi t)}{15\sqrt{3}\pi} - \frac{\cos(4\pi t)}{\sqrt{3}} + \frac{1}{\sqrt{3}}.$$

In Fig. 7(c), we compare $\eta_2(t)$ of the exact function (solid line) with the Fourier approximation (dashed line). The Laplace transforms of $\eta_j(T-t)$ are given by

$$\begin{aligned} \tilde{\eta}_1(s) &= \mathcal{L}[\eta_1(T-t)] = \sqrt{\frac{2}{3}} \frac{1}{s} - \sqrt{\frac{2}{3}} \frac{s}{s^2 + 4\pi^2}, \\ \tilde{\eta}_2(s) &= \mathcal{L}[\eta_2(T-t)] = -\frac{s}{\sqrt{3}(s^2 + 16\pi^2)} - \frac{32}{3\sqrt{3}(s^2 + 4\pi^2)} \\ &\quad + \frac{32}{5\sqrt{3}(s^2 + 36\pi^2)} + \frac{1}{\sqrt{3}s}, \end{aligned}$$

where \mathcal{L} is the Laplace transform operator. From Eq. (5), the Laplace transform of optimal linear response function $h_i(t)$ (i.e., the transfer function) is given by Eq. (14). $\tilde{h}_i(s)$ of Eq. (14) fits into the form of Eq. (D5) since Λ_i and λ_{ij} are real values.

We next show explicit representations of \mathbf{A} and \mathbf{b} which are realizations of optimal linear response functions $h_i(t)$ ($h_1(t)$ and $h_2(t)$ in Fig. 5(a)). We use \mathbf{A}_i and \mathbf{b}_i to represent \mathbf{A} and \mathbf{b} of the i th decoder:

$$\mathbf{A}_1 = \begin{bmatrix} 0.0 & 0.0 & 0.0 & 0.0 & 0.0 & 0.0 & 0.0 \\ 10.0 & 0.0 & 0.0 & 0.0 & 0.0 & 0.0 & -22.15 \\ 0.0 & 10.0 & 0.0 & 0.0 & 0.0 & 0.0 & 0.0 \\ 0.0 & 0.0 & 10.0 & 0.0 & 0.0 & 0.0 & -76.37 \\ 0.0 & 0.0 & 0.0 & 10.0 & 0.0 & 0.0 & 0.0 \\ 0.0 & 0.0 & 0.0 & 0.0 & 10.0 & 0.0 & -55.27 \\ 0.0 & 0.0 & 0.0 & 0.0 & 0.0 & 10.0 & 0.0 \end{bmatrix}, \quad (\text{D7})$$

$$\mathbf{b}_1 = [3.78 \ 1.50 \ 2.32 \ 1.13 \ 0.35 \ 0.11 \ 0.0]^\top, \quad (\text{D8})$$

$$\mathbf{A}_2 = \begin{bmatrix} 0.0 & 0.0 & 0.0 & 0.0 & 0.0 & 0.0 & 0.0 \\ 10.0 & 0.0 & 0.0 & 0.0 & 0.0 & 0.0 & -22.15 \\ 0.0 & 10.0 & 0.0 & 0.0 & 0.0 & 0.0 & 0.0 \\ 0.0 & 0.0 & 10.0 & 0.0 & 0.0 & 0.0 & -76.37 \\ 0.0 & 0.0 & 0.0 & 10.0 & 0.0 & 0.0 & 0.0 \\ 0.0 & 0.0 & 0.0 & 0.0 & 10.0 & 0.0 & -55.27 \\ 0.0 & 0.0 & 0.0 & 0.0 & 0.0 & 10.0 & 0.0 \end{bmatrix}, \quad (\text{D9})$$

$$\mathbf{b}_2 = [2.25 \ -7.80 \ 7.93 \ -5.88 \ 2.05 \ -0.60 \ 0.0]^\top. \quad (\text{D10})$$

As denoted above, these realizations are not unique, as any coordinate transformation yields the same transfer function. Thus we applied some scaling matrix to adjust excessively large values in Eqs. (D7)–(D10), which seem to be biologically infeasible. We constructed a reduced realization for the full network of Fig. 6(a). \mathbf{A}'_1 and \mathbf{b}'_1 , which are \mathbf{A} and \mathbf{b} of the reduced network, are given by

$$\mathbf{A}'_1 = \begin{bmatrix} 0 & 0 & 0 \\ 1.0 & 0 & -39.50 \\ 0 & 1.0 & 0 \end{bmatrix}, \quad (\text{D11})$$

$$\mathbf{b}'_1 = [67.40 \ 2.52 \ 0]^\top. \quad (\text{D12})$$

Network representations of Eqs. (D7)–(D12) are shown in Figs. 6(a), (c), and (e) in the main text, where positive and negative elements in \mathbf{A} and \mathbf{b} are described by activation (arrow) and inhibition (bar-headed arrow), respectively.

-
- [1] M. Behar and A. Hoffmann, *Curr. Opin. Genetics Dev.* **20**, 684 (2010).
- [2] J. E. Purvis and G. Lahav, *Cell* **152**, 945 (2013).
- [3] T. J. Kobayashi, *Phys. Rev. Lett.* **104**, 228104 (2010).
- [4] M. Hinczewski and D. Thirumalai, *Phys. Rev. X* **4**, 041017 (2014).
- [5] N. B. Becker, A. Mugler, and P. R. ten Wolde, *Phys. Rev. Lett.* **115**, 258103 (2015).
- [6] H. Kubota, R. Noguchi, Y. Toyoshima, Y.-i. Ozaki, S. Uda, K. Watanabe, W. Ogawa, and S. Kuroda, *Mol. Cell* **46**, 820 (2012).
- [7] R. Noguchi, H. Kubota, K. Yugi, Y. Toyoshima, Y. Komori, T. Soga, and S. Kuroda, *Mol. Syst. Biol.* **9**, 664 (2013).
- [8] T. Sano, K. Kawata, S. Ohno, K. Yugi, H. Kakuda, H. Kubota, S. Uda, M. Fujii, K. Kunida, D. Hoshino, et al., *Sci. Signal.* **9**, ra112 (2016).
- [9] J. Selimkhanov, B. Taylor, J. Yao, A. Pilko, J. Albeck, A. Hoffmann, L. Tsimring, and R. Wollman, *Science* **346**, 1370 (2014).
- [10] F. Tostevin and P. R. ten Wolde, *Phys. Rev. Lett.* **102**, 218101 (2009).
- [11] T. Mora and N. S. Wingreen, *Phys. Rev. Lett.* **104**, 248101 (2010).
- [12] A. Mugler, A. M. Walczak, and C. H. Wiggins, *Phys. Rev. Lett.* **105**, 058101 (2010).
- [13] J. E. Purvis and G. Lahav, *Mol. Cell* **46**, 715 (2012).
- [14] A. S. Hansen and E. K. O'Shea, *Mol. Syst. Biol.* **9**, 704 (2013).
- [15] M. Behar, D. Barken, S. L. Werner, and A. Hoffmann, *Cell* **155**, 448 (2013).
- [16] S. S. Mc Mahon, O. Lenive, S. Filippi, and M. P. H. Stumpf, *J. R. Soc. Interface* **12**, 20150597 (2015).
- [17] H. K. Makadia, J. S. Schwaber, and R. Vadigepalli, *PLoS Comput. Biol.* **11**, e1004563 (2015).
- [18] W. de Ronde, F. Tostevin, and P. R. ten Wolde, *Phys. Rev. Lett.* **107**, 048101 (2011).
- [19] W. de Ronde and P. R. ten Wolde, *Phys. Biol.* **11**, 026004 (2014).
- [20] R. G. Gallager, *Information theory and reliable communication*, vol. 2 (Springer, 1968).
- [21] K. Wang, W.-J. Rappel, R. Kerr, and H. Levine, *Phys. Rev. E* **75**, 061905 (2007).
- [22] C. C. Govern and P. R. ten Wolde, *Phys. Rev. Lett.* **109**, 218103 (2012).
- [23] M. Marhl, M. Perc, and S. Schuster, *Biophys. Chem.* **120**, 161 (2006).
- [24] Y. Hasegawa and M. Arita, *J. R. Soc. Interface* **11**, 20131018 (2014).
- [25] Y. Hasegawa and M. Arita, *Phys. Rev. Lett.* **113**, 108101 (2014).
- [26] Y. Hasegawa, *New J. Phys.* **18**, 113031 (2016).

- [27] R. L. Williams and D. A. Lawrence, *Linear state-space control systems* (John Wiley & Sons, 2007).
- [28] S. Mangan and U. Alon, Proc. Natl. Acad. Sci. U.S.A. **100**, 11980 (2003).
- [29] U. Alon, *An Introduction to Systems Biology* (CRC Press, 2007).
- [30] J. M. R. Parrondo, J. M. Horowitz, and T. Sagawa, Nat. Phys. **11**, 131 (2015).
- [31] P. Sartori, L. Granger, C. F. Lee, and J. M. Horowitz, PLoS Comput. Biol. **10**, e1003974 (2014).
- [32] A. C. Barato, D. Hartich, and U. Seifert, New J. Phys. **16**, 103024 (2014).
- [33] T. E. Ouldridge, C. C. Govern, and P. R. ten Wolde, Phys. Rev. X **7**, 021004 (2017).